Biobased hydrogel nanocomposite reinforced with wastepaper-derived modified cellulose nanofiber

Highlights

This chapter illustrates the fabrication process of modified-cellulose nanofiber (mCNF) incorporated biobased hydrogel nanocomposite (HNC) and its utilization as an efficient adsorbent for cationic dye removal. This work involved the preparation of cellulose nanofiber (CNF) from wastepaper by applying different processes such as alkali, acid, bleaching and DMSO treatments. Further, the CNF was treated with sodium monochloroacetate to produce mCNF. The results indicated that the modification of CNF improved its interaction with the hydrogel matrix, leading to enhanced water absorption as well as the dye removal capacity of the HNC. Further, the adsorption/desorption and mixed dye removal tests were performed to investigate the dye removal ability of HNC, and the results clearly revealed that it can be used as an effective and reusable adsorbent for removal of different cationic dyes from wastewater.

Parts of this chapter are published as

[1] Bora, A. and Karak, N. Biobased hydrogel reinforced with wastepaper-derived modified cellulose nanofiber as an efficient dye remover from wastewater. *Journal of Polymer Research*, 30(12):452, 2023.

4.1. Introduction

Over the past few years, contaminations by waste dyes have created a serious environmental problem because of their continuous introduction from different industries such as textiles, printing and dying, cosmetics, etc. into the water bodies. Dyes containing azo and aromatic groups are accountable for a tremendous increase in environmental deterioration because of their non-degradable and highly toxic in nature [1,2]. Their presence of even at very low concentrations can have adverse effects on human health and on the surroundings. In order to inhibit those harmful effects, it is necessary to treat dye-contaminated water before its release into the environment. As discussed in **Chapter 1,** several research works on the fabrication of biobased hydrogel nanocomposites (HNCs) reinforced with various nanomaterials (NMs) including metals, metal oxides, clays, etc. have been carried out for the removal of dyes from wastewater in terms of their cost-effectiveness and excellent efficiency even at very low concentrations. HNCs possess improved properties including water swelling, adsorption capacity, etc. because of which it can be able to remove a huge amount of dye molecules effectively. Moreover, the introduction of NMs can increase the surface area to volume ratio, which in turn creates additional adsorption sites for dye molecules on HNCs surface [3,4]. Currently, cellulose-based NMs such as cellulose nanofibers (CNFs), cellulose nanowhiskers (CNWs), cellulose nanocrystals (CNCs), etc. have been gaining extensive interest from researchers and industrialists due to their abundant, renewable, and biodegradable properties [3]. They possess excellent reinforcing capability due to the existence of β-(1,4) glycosidic linkages and hydroxyl groups that enable the hydrogen bonds which improves properties of polymers [5]. Moreover, cellulose can be obtained from many sources, including banana rachis, wood, sisal, etc. [6]. However, it is advantageous to use waste materials instead of fresh plant sources for isolation of cellulose. As described in **Chapter 3**, wastepaper (WP) as the raw material for isolation of CNF can be served as a potential source of cellulose which do not need to be further processed physically or chemically to remove hemicellulose and lignin. It has been found that most of the hemicellulose and lignin are already extracted throughout the papermaking process [7].

Therefore, the purpose of this work is to develop a biobased hydrogel nanocomposite (HNC) with incorporation of WP derived modified-CNF (mCNF) as the reinforcing agent for the elimination of dyes from the contaminated aqueous media. Moreover, to

increase the amount of biocomponent of the hydrogel, biobased raw materials i.e., starch and itaconic acid (IA) were used, but a little synthetic monomer like acrylic acid (AA) was also used to improve the performance of the hydrogel. Further, we carried out the surface modification of CNF which was used as a nano-reinforcing agent to enhance the water absorption capacity (WAC) and to improve dye removal efficiency of the hydrogel. The structures of mCNF and the prepared HNCs were characterized through various spectroscopic and microscopic techniques. Adsorption kinetics and equilibrium adsorption isotherms for methylene blue (MB), methyl violet (MV), malachite green (MG) and cresol red (CR) dyes onto mCNF treated hydrogel were also investigated for understanding adsorption mechanism of the combined hydrogel matrix and mCNFs system.

4.2. Experimental section

4.2.1. Materials

Various chemicals including starch, IA, AA, ammonium persulfate (APS), N,N'-methylene bis-acrylamide (MBA), and NaOH were used with similar quality and specifications as mentioned in **Chapter 2.** Further, WP of the same quality and characters are also used to isolate CNFs as those described in **Chapter 3**.

Glacial acetic acid (molar mass 60.05 g/mol), dimethyl sulfoxide (DMSO) (molar mass 78.13 g/mol), and hydrogen peroxide (H_2O_2) (molar mass 34.01 g/mol) were purchased from Merck, India and used as pretreatment agents for CNF isolation.

Sodium monochloroacetate (SMCA) (molar mass 116.48 g/mol) was supplied by Sigma-Aldrich, Germany and utilized for modification of CNFs.

Cationic dyes including MB (molar mass 319.85 g/mol), MG (molar mass 364.91 g/mol), MV (molar mass 407.97 g/mol), and CR (molar mass 404.41 g/mol) were used as model organic pollutant for dye adsorption test. MB was supplied by LOBA Chemie, India. MG and MV were purchased from SRL, India. CR was provided by Sigma-Aldrich, Germany.

4.2.2. Preparation of CNF

The CNF was isolated from WP obtained from the laboratory by using the method reported by Mandal and Chakrabarty with some modifications [8]. Initially, WP was collected from our laboratory and washed with 0.5% NaOH solution followed by washing with distilled water until pH became neutral and dried in an oven at 60 ℃.

Then, 2.5 g of dried paper was grounded in a mixture-grinder and placed into a 250 mL three-necked round bottom (RB) flask. Subsequently, these grounded papers were treated with 100 mL 5 wt% NaOH solution (paper to liquor ratio of 1:40 Vol/Vol) by continuous stirring (using a mechanical stirrer) at 70 ℃ for 2.5 h followed by washing with distilled water until a neutral pH was reached. In the next step, acid hydrolysis was conducted where the residue was treated with 75 mL 50% (Vol/Vol) glacial acetic acid by continuous stirring at 65 ℃ for 2.5 h and it was washed again as before. Further, the residue was bleached using 50 mL 7% (Vol/Vol) H_2O_2 (bleaching agent) at 50 ℃ for 2 h and the residue was neutralized with water. In the final step, treatment with 50% DMSO was carried out for another 2.5 h at 70 ℃. After completion of the step, the residue was washed with water and centrifuged at 3500 RPM for 10 min to separate DMSO from the isolated cellulose fibers. The centrifugation process was continued to complete the removal of DMSO from the fibers. Then, the fibers were mechanically dispersed in water using a probe ultrasonicator (UPS200) for 10 min in an ice bath to avoid overheating to obtain a suspension of CNF.

4.2.3. Surface modification of CNF

The modification of CNF was conducted in water according to the method outlined by Alam *et al*. with some modifications [9]. Initially, the CNFs were suspended in water (2% wt/Vol) containing SMCA (fiber to SMCA ratio 1:2 wt/wt) in a three neck RB flask at room temperature for 10-15 min. Then, the temperature was raised to 45 ℃ for 30 min to permit the penetration of SMCA into the fiber core and subsequently, the pH of the mixture was adjusted by addition of 2% wt/Vol NaOH and agitated for 10-15 min. Thereafter, the reaction was conducted at 45 ℃ for 6 h. Upon completion of the reaction, the obtained fibers were washed with distilled water, and it was dispersed in water with the help of an ultrasonicator. Finally, 0.01, 0.05 and 0.1 wt% of mCNF aqueous dispersions were prepared and used for further studies.

4.2.4. Yield of mCNF

The yield of mCNF fraction was calculated using the following equation [10].

$$\text{Yield (\%)} = \frac{Weight\ of\ dried\ mCNF}{weight\ of\ dried\ CNF} \times 100 \text{----------} \textbf{(Eq. 4.1)}$$

4.2.5. Preparation of HNC

In this work, best formulation chosen from **Chapter 2** was selected for fabrication of HNCs and it was prepared by mixing with mCNF into the hydrogel matrix using the same method as described in the chapter with some modifications. Initially, starch was gelatinized in 10 mL of 0.067N NaOH solution in the presence of IA by stirring at 80-90 ℃ in a three-neck RB flask, that was equipped with a mechanical stirrer. Thereafter, temperature of the reaction mixture was reduced to 60 ℃ and AA mixed with 1 mL of water and different concentrations of mCNFs (0, 0.01, 0.05 and 0.1 wt% with respect to total solid components) or unmodified CNFs dispersions were gradually poured into the flask. Afterward, MBA mixed with APS in water (1 mL) and was added into the reaction mixture. Thereafter, it was allowed to polymerize at 70 ℃ for 1.5-2 h under the nitrogen environment. After formation of solid like substance, it was allowed to cool down to room temperature. Further, the obtained hydrogel was immersed in 50 mL of alkaline solution (0.3 N) to neutralize the remaining carboxyl groups as well as to enhance adsorption capacity of the hydrogel. In the subsequent step, the neutralized hydrogels were washed with water and immersed in distilled water for 24 h to get swollen hydrogel which were teared into small pieces using mechanical stirrer and washed with methanol to replace the absorbed water from hydrogel. Then, white solid type substance was obtained which were dried at 60 ℃ in a hot air oven until a fixed weight was reached. In the end, dried hydrogels were grounded into fine powder which were applied for further studies. The prepared HNCs are coded according to their compositions as given in **Table 4.1**.

Table 4.1. Compositions of the synthesized HNCs.

Sample code	Starch (g)	IA (g)	AA (g)	MBA (g)	APS (g)	CNF (wt%)	mCNF (wt%)
H-0	1	0.1	0.9	0.01	0.04	0	0
H-1	1	0.1	0.9	0.01	0.04	0.01	0
H-2	1	0.1	0.9	0.01	0.04	0.05	0
H-3	1	0.1	0.9	0.01	0.04	0.10	0
H-4	1	0.1	0.9	0.01	0.04	0	0.01
H-5	1	0.1	0.9	0.01	0.04	0	0.05
H-6	1	0.1	0.9	0.01	0.04	0	0.10

4.2.6. Structural analysis

Details of various spectroscopic, analytical, and microscopic instruments including FTIR, TGA, XRD and SEM are the same as mentioned in **Chapter 2** and **Chapter 3.** The crystallinity index (C.I.) was determined from the XRD diffractograms using the following equation [9].

$$\text{C.I. (\%)} = \frac{I_{200} - I_{AM}}{I_{200}} \times 100 \text{ ----------(Eq. 4.2)}$$

where I_{200} represent the maximum peak intensity corresponding to (200) plane and I_{AM} is the minimum intensity between the peaks corresponding to (110) and (200) planes. Further, the dye adsorption study was investigated using the same UV spectrophotometer as mentioned in **Chapter 3**.

Moreover, the morphology of the CNF was characterized using FEI company, USA transmission electron microscope (TEM) (TECNAI G2 20 S-TWIN (200KV)). DLS measurement of aqueous dispersion of mCNF was performed using particle analyzer (Nanoplus-3) to measure the particle size. The Nano ZS Zetasizer (Malvern) instrument was used to measure the zeta potential of the samples.

4.2.7. Water swelling test

To measure the equilibrium WAC of the synthesized HNCs, **Eq. 2.1.** of **Chapter 2** was used as described in that chapter.

4.2.8. Dye adsorption test

In this work, the dye adsorption studies were carried out using powdered hydrogel samples. The adsorption tests were performed in 100 mL of plastic containers containing 50 mL of dye solutions by changing the adsorbent dosage (from 10 mg to 40 mg), contact time (up to 180 min) and initial concentration of dye solution (from 50 ppm to 90 ppm). The mixtures were shaken at 200 rpm at room temperature. Upon completion of the experiment, the residual concentration of dye sample was measured using the UV-visible spectrophotometer at wavelengths of 658, 575, 611 and 457 nm which corresponds to the maximum absorbance wavelength of MB, MV, MG and CR dyes, respectively. The dye adsorption capacity (q_e) of the hydrogels was calculated by using the following equation [11].

$$q_e = \frac{C_0 - C_e}{m} \text{ x V --------(Eq. 4.3)}$$

where C_0 and C_e signify the initial and final concentrations of dye solutions (mg/L), V represent the volume of dye solution (L), and m is the dry weight of hydrogel (g).

4.2.9. Kinetic models

To carry out the kinetic study, 50 mL of each dye solution was treated with 10 mg of adsorbent for the contact time of 3-120 min. To investigate the adsorption kinetics of MB, MV, MG, and CR onto hydrogels, we conducted the test with a lower dye concentration i.e., 50 ppm. The concentration of dye solution was determined spectrophotometrically by withdrawing aliquots of the dye solution at a predetermined time interval. In this work, the pseudo-first-order (PFO) and pseudo-second-order (PSO) kinetic equations were fitted into the experimental data to investigate the kinetic behavior of the hydrogel for the removal of MB, MV, MG, and CR dyes from aqueous solution. The PFO (**Eq. 4.4**) and PSO (**Eq. 4.5**) equation can be expressed as follows [11].

$$\ln(q_e - q_t) = \ln q_e - k_1 t \text{ ----------} \textbf{(Eq. 4.4)}$$

$$t/q_t = 1/(k_2 q_e^2) + t/q_e \text{ ----------} \textbf{(Eq. 4.5)}$$

where k_1 and k_2 represent the equilibrium rate constant of PFO (min^{-1}) and PSO models ($g\ mg^{-1}min^{-1}$), respectively; q_e and q_t indicate the adsorption capacity (mg/g) at equilibrium and at time (t), respectively.

4.2.10. Adsorption isotherm models

Isotherm studies were performed with different initial concentrations of dyes in the range of 40-90 ppm at fixed contact time and adsorption dosage i.e., 120 min and 10 mg. Herein, two classical models, namely, Langmuir and Freundlich adsorption isotherms were employed to evaluate the adsorption behavior of the hydrogels. The parameters of adsorption isotherms were obtained by plotting the experimental data into the two isotherm equations and best fitted isotherm was chosen based on higher correlation coefficient value [1].

The Langmuir (**Eq. 4.6**) and Freundlich (**Eq. 4.7**) adsorption isotherm models can be expressed in the following linear forms.

$$C_e/q_e = 1/(q_m K_L) + C_e/q_m \text{ ---------} \textbf{(Eq. 4.6)}$$

$$\ln(q_e) = \ln(K_F) + 1/n \ln C_e \text{ ---------} \textbf{(Eq. 4.7)}$$

where K_L and K_F are the Langmuir and Freundlich adsorption constants, and n is the heterogeneity factor, C_e (mg/L) represents dye concentration in equilibrium (mg/L), q_e (mg/g) and q_m (mg/g) represent maximum and equilibrium adsorption capacity, respectively.

4.2.11. Mixed dye adsorption

The mixed adsorption test was performed in a mixed MB/MV/MG/CR dye solution at fixed initial concentration of each dye (90 ppm). The mixed dye solution was prepared by mixing 25 mL of each dye solutions in a container, then 10 mg of dry hydrogel sample was immersed in the solution and shaken on a magnetic stirrer at 200 rpm. After the adsorption test, the solution was filtered, and the remaining amounts of dyes were measured at λ_{max} of individual dye [12].

4.2.12. Reusability experiment

In practical dye removal applications, the recovery/reusability is considered as one of the most important features of a solid adsorbent. In this work, three adsorption/desorption cycles were carried out to study the recyclability of HNC. Initially, 10 mg of dry hydrogel powder was placed in a tea bag and stirred in 50 mL of dye solution (50 ppm) for 120 min. The amount of adsorbed dye was measured with the help of a UV spectrophotometer. Then, desorption of the dye adsorbed hydrogel was conducted by immersing the tea bag in 50 mL of 0.1N HCl solution and stirring at 200 rpm for 60 min at 35 ℃. The regenerated sample was rinsed with distilled water and immersed again in NaOH solution to generate COO^- by deprotonating the COOH group present in the hydrogel. Then, the q_e value was measured after each adsorption/desorption cycle using the same equation as mentioned earlier [11].

4.3. Results and discussion

4.3.1. Isolation and modification of CNFs

Besides, hemicellulose and lignin, wastepaper contains around 5% extractives and 11% ash content, indicating the presence of resins, ink components and binders used in the papermaking process [13]. Therefore, to remove these impurities from cellulose fibers, we used different processes (such as alkali, acid, bleaching and DMSO treatment) to extract CNF from wastepaper. Initially, the deinking process was carried out to remove ink followed by alkali treatment to remove hemicellulose and lignin from the paper

material. Further, acid treatment dissolves amorphous regions of cellulose and residual hemicellulose. This process also reduces the molar mass and size of the cellulose leading to the formation of nano-sized fibers [14]. In addition, a primary bleaching treatment was applied to eliminate lignin by using hydrogen peroxide which react with carbonyl groups of lignin, resulting in the degradation of complex bonds between polysaccharides and lignin [15]. Moreover, DMSO is considered as a potential pretreatment agent as it is a suitable solvent for hemicellulose as well as DMSO has been proved to swell cellulose microfibrils by breaking the inter- and intra-molecular H-bonds of the remaining lignocellulosic materials [16]. Further, CNFs were modified via etherification of primary hydroxyl group of cellulose using SMCA under alkaline condition and yield of about 60% was obtained for mCNF. In **Scheme 4.1**, the process of isolation of CNFs and its modification is shown. From this scheme it is observed that, CNF dispersion becomes more stable after its modification. This can be attributed to the presence of negatively charged carboxylate groups on the surface of mCNF which in turn leads to the generation of electrostatic repulsion between fibers that make the dispersion more stable [17].

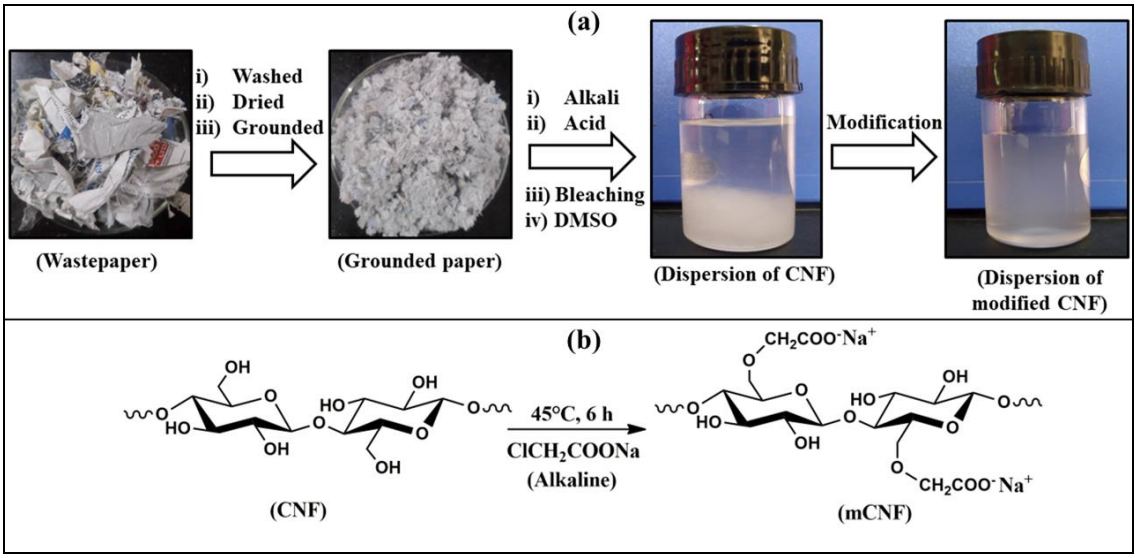

Scheme 4.1. (a) Graphical illustration of isolation of CNF from WP and (b) schematic representation of modification of CNF.

4.3.2. Preparation of the HNCs

The HNCs were prepared by graft copolymerization of AA and IA onto starch backbone in the presence of crosslinking agents (MBA) and by subsequent incorporation of reinforcing agent (mCNF). The schematic illustration of formation of HNC is shown in **Scheme 4.2**. Firstly, upon heating of APS initiator, sulfate anion-radicals are generated,

which in turn abstract hydrogen from the primary hydroxyl groups present in the starch and leads to the formation of alkoxy radicals. Then the monomer molecules (AA and IA) become acceptors of alkoxy radicals and start propagation of a new polymeric chain. Thereafter, the two end vinyl groups of MBA react simultaneously with the polymeric chain which in turn leads to the formation of three-dimensional (3D) cross-linked structure, as shown in **Scheme 4.2.** [18].

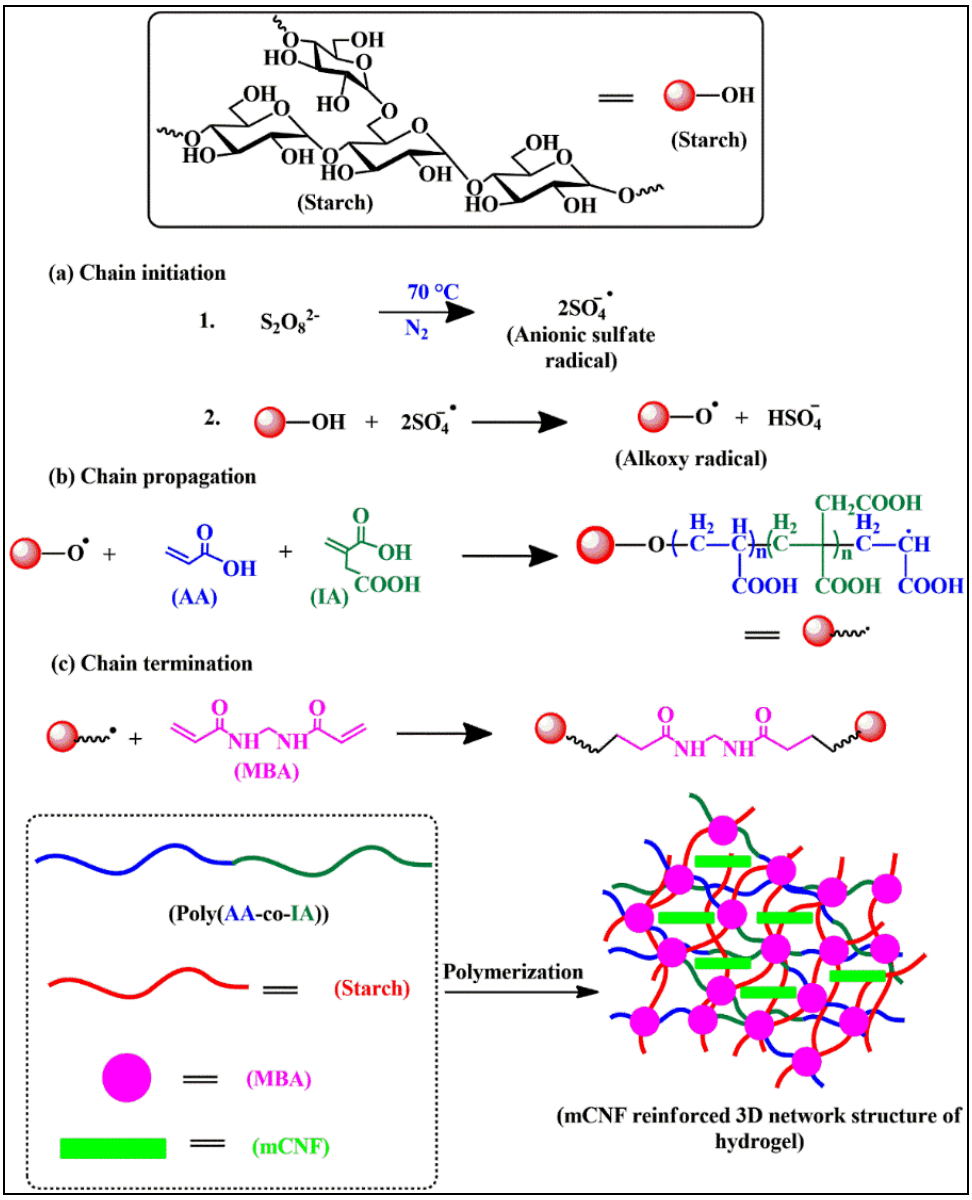

Scheme 4.2. Schematic illustration of fabrication of mCNF reinforced HNCs.

4.3.3. Characterization

4.3.3.1. FTIR

FTIR spectra of CNF and mCNF are analyzed and shown in **Figure 4.1.a**. The characteristic peak at 3390 cm^{-1} is attributed to the stretching vibrations of –OH groups.

A distinctive peak at 1636 cm^{-1} represents the bending vibration mode of –OH group of the absorbed water [19]. The absorption bands that belong to the vibrations at 1058 cm^{-1} indicates the cellulosic β-1,4-glycosidic bond. Two peaks around 2908 cm^{-1} and 1446 cm^{-1} are corresponding to the CH bending and stretching modes. These two peaks indicating the presence of glucose units of the polysaccharide. The characteristic absorption peaks of mCNFs were basically consistent with those of the CNFs. Moreover, it was worth noting that a new peak appeared at 1720 cm^{-1} in mCNF has supported that CNF was successfully modified via carboxymethylation reaction [20].

From the FTIR spectra of HNCs, it is observed that the absorption bands of the prepared HNCs are almost similar to each other which are depicted in **Figure 4.1.b.** The typical peaks of the hydrogels at around 3448, 2916 and 2854 cm^{-1} are ascribed to the stretching vibration peaks of −OH, the asymmetric and symmetric stretching vibrations of aliphatic C–H groups, respectively. The peak at 1727 cm^{-1} associated with the stretching vibration of carbonyl group present in carboxyl groups (COOH) is appeared because of the graft copolymerization of AA and IA onto CS. The peak at 1012 cm^{-1} indicates the ether linkage of the starch moiety. Thus, from the above FTIR analysis, formation of mCNF from CNF and the structure of the prepared hydrogels can be supported [3,21].

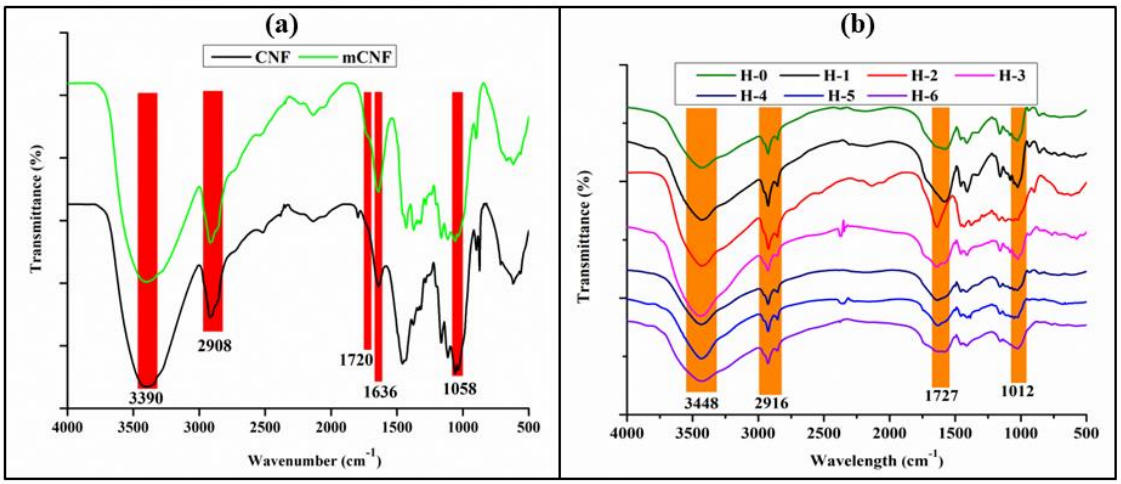

Figure 4.1. FTIR spectra of (a) CNF and mCNF, and (b) HNCs.

4.3.3.2. TGA analysis

In this study, both TGA and DTG profiles of CNF, mCNF, H-0, H-3 and H-6 were analyzed in the temperature range of 30–600 ℃ which are depicted in **Figure 4.2**.(**a-d**), respectively. Due to the evaporation of water, an initial weight loss was observed for CNF, mCNF H-0, H-3 and H-6 at temperature below 260 ℃. A second degradation

region between 214-399 °C was also observed due to the generation of volatile products [22]. The second degradation temperature of CNF was observed from 263 to 389 °C with a weight loss of 50% from its initial weight, while mCNF started to decompose earlier within the temperature range of 214–367 °C with 60% weight loss which is higher as compared to CNF. For H-0, H-3 and H-6, the second degradation stage took place at a temperature range of 233–399 °C. The percent weight loss of mCNF was higher compared to CNF which can be attributed to the evolution of CO_2 produced by decarboxylation and decomposition of cellulose backbone [23]. Meanwhile, for HNCs, third stage of weight loss was observed in the range of 410-524 °C which can be ascribed to the breakdown of the crosslinked polymer network [22]. From the DTG curves, it was observed that CNF showed the highest maximum degradation temperature (T_{max}) at 365 °C compared to mCNF at 331 °C. This can be ascribed to the well-ordered, highly crystalline structure of CNF, which makes it thermally more stable than mCNF. Since the modification affected the molecular structure of CNF and its bonding energy, thereby disrupting the crystallinity, mCNF starts to decompose earlier than CNF. This statement is in great agreement with the results obtained from XRD analysis which is explained in the following section. Moreover, the T_{max} of H-3 and H-6 was found at around 300 °C, which is higher than the T_{max} of H-0 observed at 292 °C, it can be ascribed to a high thermal stability of H-3 and H-6 compared to bare hydrogel due to the incorporation of prepared reinforcing agents into the hydrogel matrix [21,24].

4.3.3.3. XRD analysis

The XRD profiles of CNF, mCNF, untreated hydrogel (H-0), CNF treated hydrogel (H-3) and mCNF treated hydrogel (H-6) are shown in **Figure 4.3**. The C.I. was calculated to understand the alterations in the degree of crystallinities in CNF, mCNF and HNCs. The strong diffraction peaks at 16.41° and 22.83° were observed, which are the characteristic peaks for cellulose I type [20]. From **Figure 4.3.a**, the XRD pattern of CNF shows three peaks at 2θ=15.7°, 22.51°, and 34.11°, which are corresponds to the 110, 200, and 004 planes, respectively [19]. The C.I. of the unmodified CNF was determined to be 71%. However, the C.I. of mCNF was found to be 60%. Thus, it can be observed that C.I. of CNF was higher indicating the presence of more crystalline phases in CNF compared to mCNF. The loss of crystallinity is probably due to the substitution of surface hydroxyl groups with the SMCA under alkaline condition during carboxymethylation, which weakens the H-bonding between cellulose fibers, thereby disrupting the well-ordered

crystalline structure [24]. These results are supported by the TGA data, which established that mCNF has a lower T_{max} compared to CNF due to the loss of the crystallinity [20].

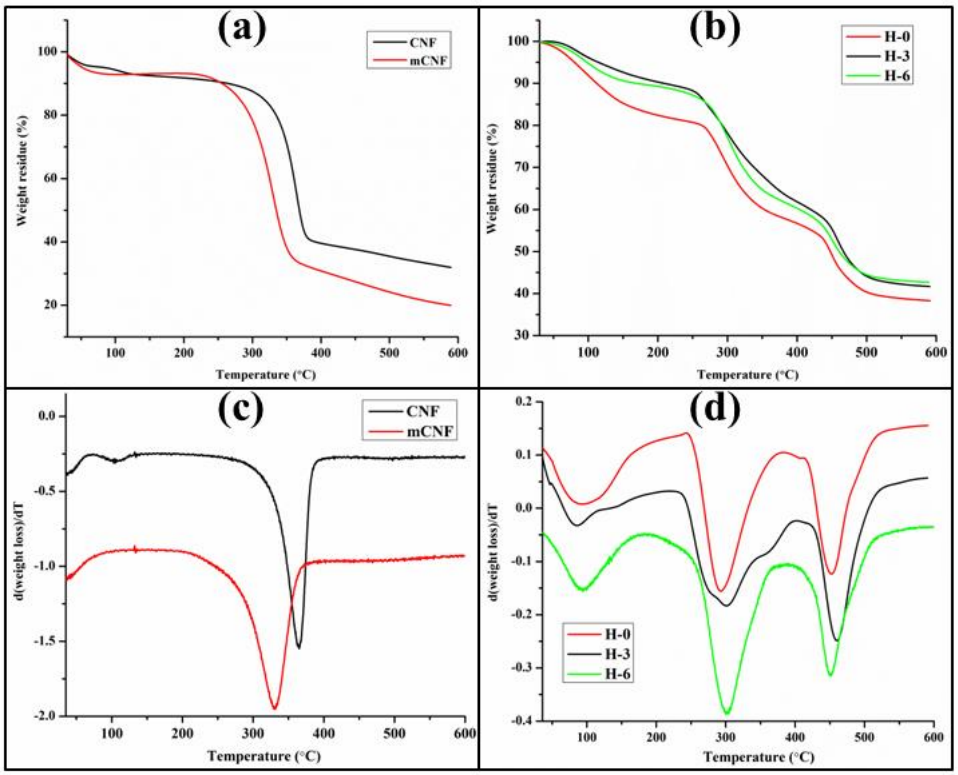

Figure 4.2. TGA thermograms of (a) CNF and mCNF; and (b) HNCs (H-0, H-3, H-6) and DTG curves of (c) CNF and mCNF; and (d) HNCs (H-0, H-3, H-6).

Again, from **Figure 4.3.b**, the presence of broad and faint peaks denotes the amorphous nature of the HNCs. However, the typical peak intensity of HNCs at 2θ=22° has considerably increased after the addition of CNF and mCNF in the case of H-3 and H-6, respectively. Thus, by comparing the XRD patterns of H-0, H-3 and H-6, it is possible to confirm that CNF and mCNF were successfully incorporated within the hydrogel network [19].

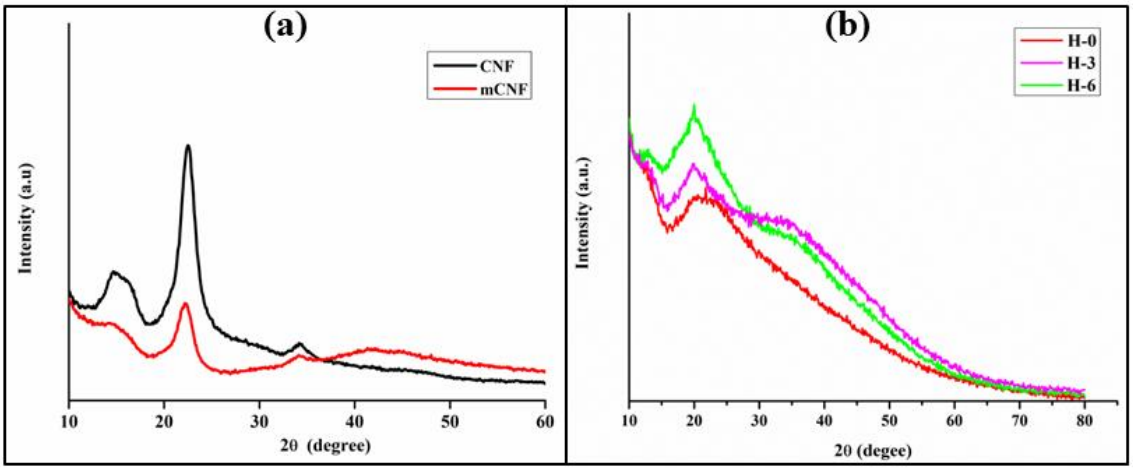

Figure 4.3. XRD patterns of (a) CNF, mCNF; and (b) HNCs (H-0, H-3, H-6).

4.3.3.4. Transmission electron microscope (TEM)/ Dynamic light scattering (DLS)/ Zeta potential analysis

To study the shape and morphology as well as the size distribution of prepared reinforcing agents, TEM and DLS studies were carried out. The TEM images of mCNF are shown in **Figure 4.4.a**, from which, the formation of wire-like cellulose nanofibers with nanoscale width can be confirmed after the modification of CNFs. This result is consistent with those from the DLS results. The results showed that the particle size distribution of obtained mCNFs with diameter in the range of 68-270 nm (**Figure 4.4.b**). In contrast, the particle size distribution of CNFs was found in a higher diameter in the range of 60 to 550 nm as compared with mCNF (**Figure 4.4.c**). Moreover, the zeta potential revealed the higher stability of CNF after modification. The zeta potential of CNF was found to be -19.2 mV (**Figure 4.5.a**), while that of mCNF was found to be more negative, i.e., -29.3 mV (**Figure 4.5.b**). The modification of CNF increased the surface charge of mCNF, resulting in more electrostatic repulsion between the modified nanofibers, which improved their stability in water compared with unmodified fibers.

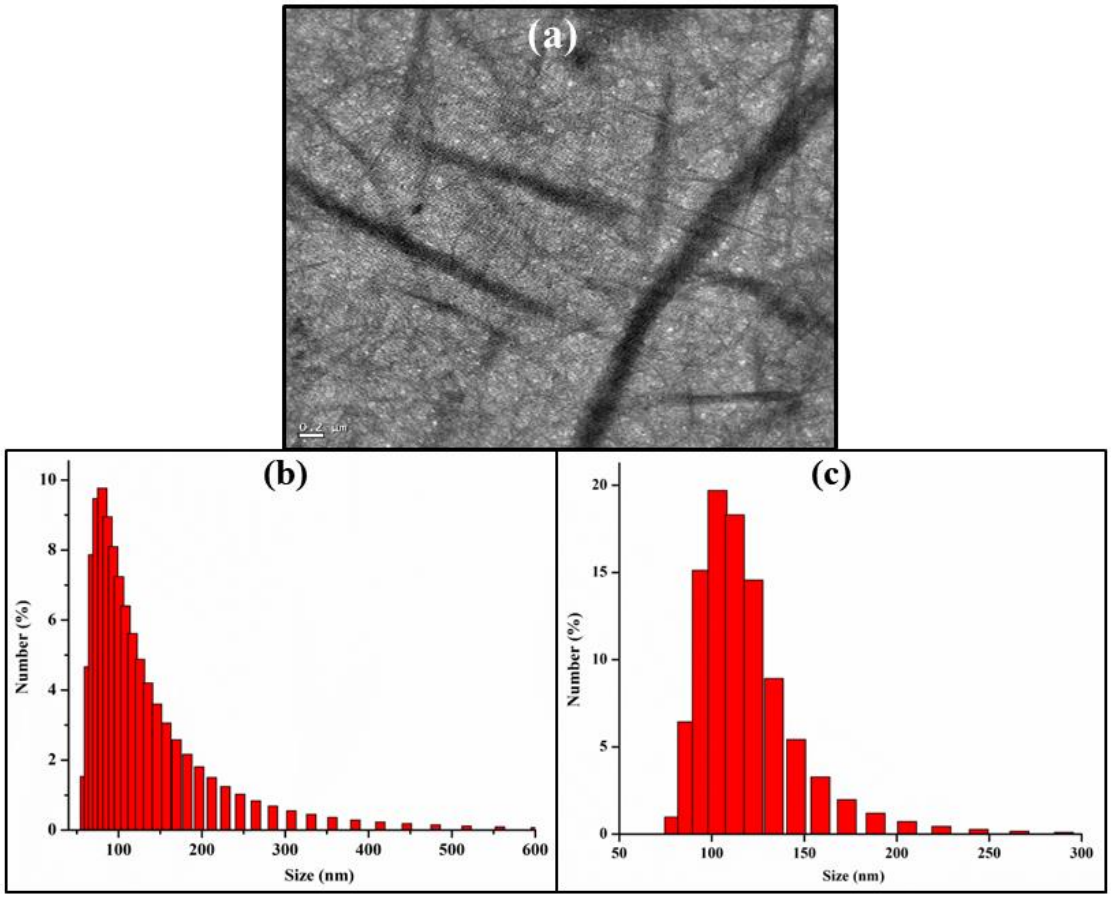

Figure 4.4. (a) TEM image of mCNF (scale bar is 0.2 µm). Particle size distribution of (b) CNF and (c) mCNF measured with DLS.

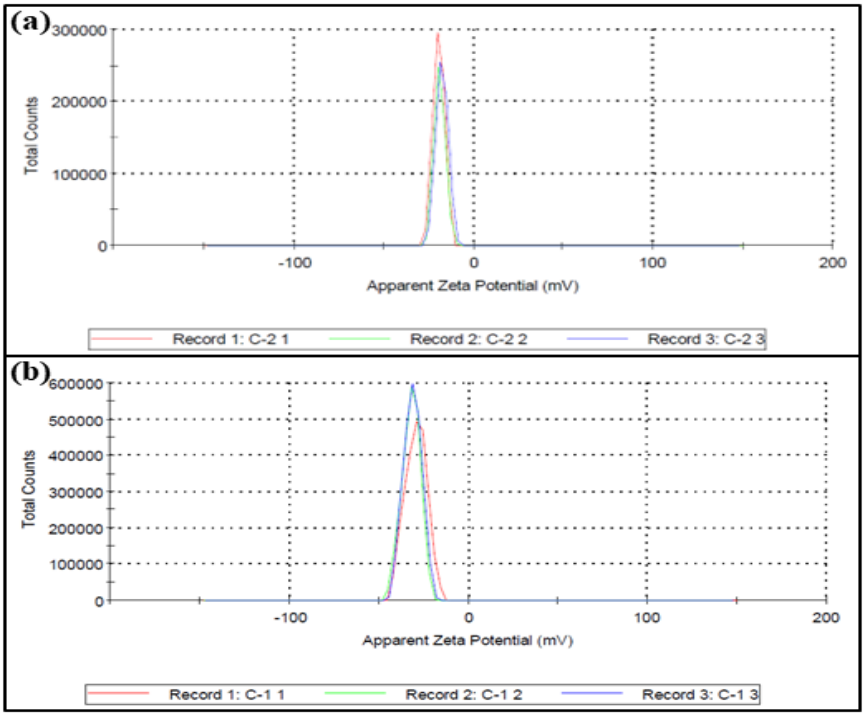

Figure 4.5. Zeta potential of (a) CNF and (b) mCNF.

4.3.3.5. SEM analysis

The surface morphological features of bare hydrogel (H-0), CNF incorporated hydrogel (H-3) and mCNF-loaded best water absorbing hydrogel (H-6), were investigated using SEM images which are shown in **Figure 4.6**. As depicted by the figure, a significant difference was not observed in the number and distribution of the pores present in the polymeric matrices. A porous surface morphology was observed in all the compositions which can be accredited to the formation of a three-dimensionally cross-linked polymeric structure [1]. The presence of numerous pores on H-0, H-3 and H-6 explains their excellent water absorption and dye adsorption capacities.

4.3.3.6. Swelling property of HNC

It is considered that swelling capacity is an important property of adsorbents which effects on the removal capacity towards dyes and metal ions [25]. Therefore, the equilibrium WAC of the synthesized HNCs were investigated in distilled water and the results are shown in **Figure 4.7**. The obtained results showed that swelling capacity of the hydrogel treated with CNF was higher than that of the untreated hydrogel (**Figure 4.7.a**). It was also observed that the swelling capacity of HNC increased with increasing CNF content and maximum WAC (656 g/g) was obtained as compared to hydrogel without CNF i.e., 507 g/g, which could be attributed to the increased hydrophilicity of the hydrogel matrix due to the presence of OH groups on the surface of CNFs.

Additionally, the uniform distribution of CNF in the hydrogel matrix inhibits the polymer chains from becoming entangled, leading to a decrease in physical cross-linking density in the hydrogel network, leading to an increase in the water swelling capacity.

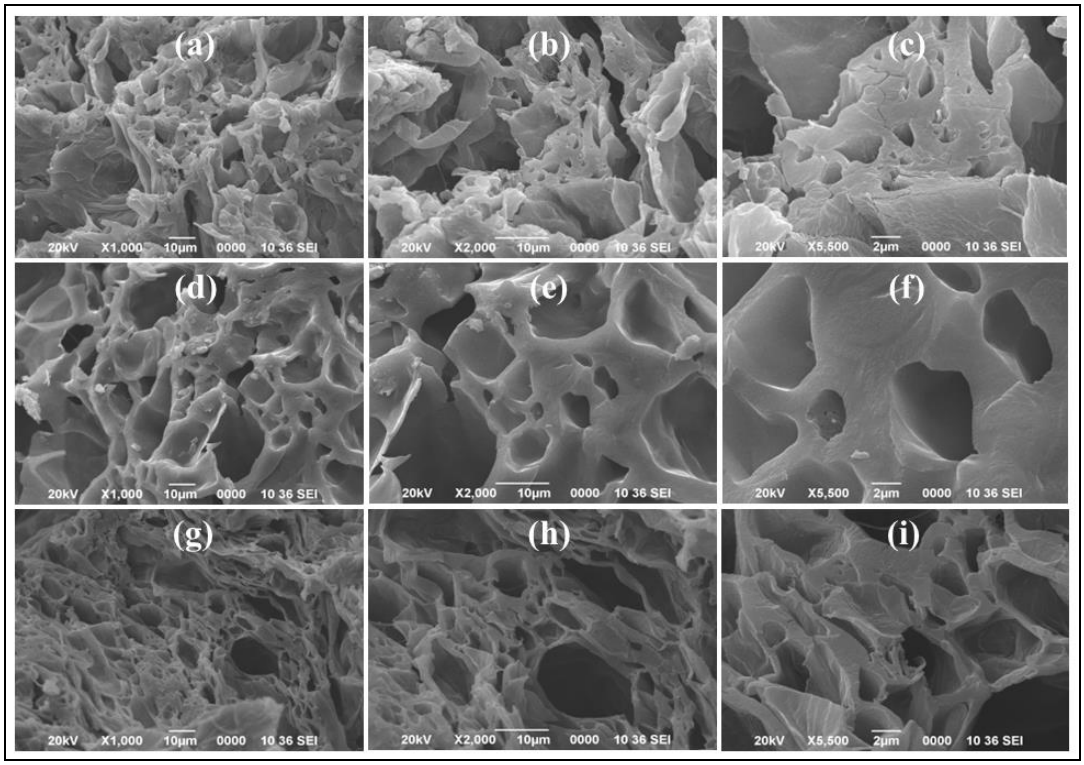

Figure 4.6. Morphological images of H-0 (a-c), H-3 (d-f) and H-6 (g-i) at 1000, 2000 and 5500X magnifications.

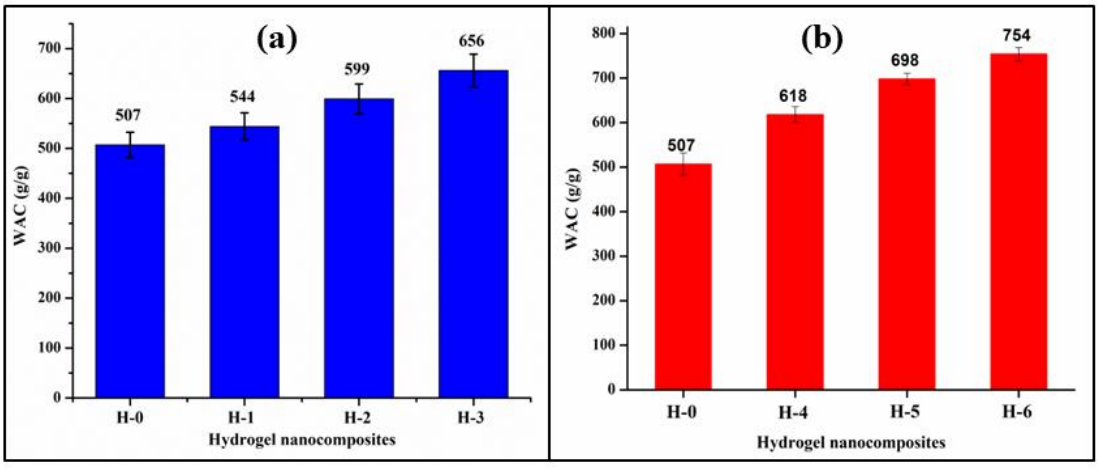

Figure 4.7. Effect of (a) CNF and (b) mCNF content on WAC of the prepared HNC.

Moreover, enhanced water swelling capacity was also observed in the case of mCNF incorporated HNCs (754 g/g) with mCNF content of 0.1 wt% which is observed to be 48% greater than the equilibrium WAC of hydrogel without mCNF (507 g/g) (**Figure 4.7.b**). This positive change can be credited to the existence of hydrophilic groups (OH and COO^-) on the mCNFs surface which increased the electrostatic repulsion within the

hydrogel network structure which in turn generate more osmotic pressure differences. It is found that when the osmotic pressure difference is larger, the permeation of water inside the absorbents become faster. Moreover, polymeric chains are inhibited from intertwining due to the presence of mCNF nanofillers and thus, cross-linking density of the hydrogel network decreases, which in turn results in high water absorption by mCNF treated hydrogel [26].

4.3.3.7. Dye adsorption with oven dried hydrogels

For the purpose of investigating the adsorption of dyes on prepared HNCs, cationic dyes like MB, MG, MV and CR were chosen as model dye pollutants to explore their adsorption on the prepared HNCs. For comparison, the q_e of CNF and mCNF treated hydrogels and untreated hydrogel are depicted in **Figure 4.8.a**. Moreover, the effect of the mCNFs content on the q_e value of the hydrogel is also depicted in **Figure 4.8.b**. As shown in **Figure 4.8.a**, the q_e of H-3 reinforced with 0.1 wt% CNF content was found to be 318±16, 300±15, 297±14 and 244±12 $mg \cdot g^{-1}$ for MB, MV, MG and CR, respectively which is higher in comparison with the untreated counterpart indicating the introduction of CNFs enhanced the cationic dye adsorption ability of H-3 hydrogel. It may be due to the high surface area of CNFs and the existence of numerous hydroxyl groups in cellulose structure which in turn generate more sorption sites for removal of cationic dyes.

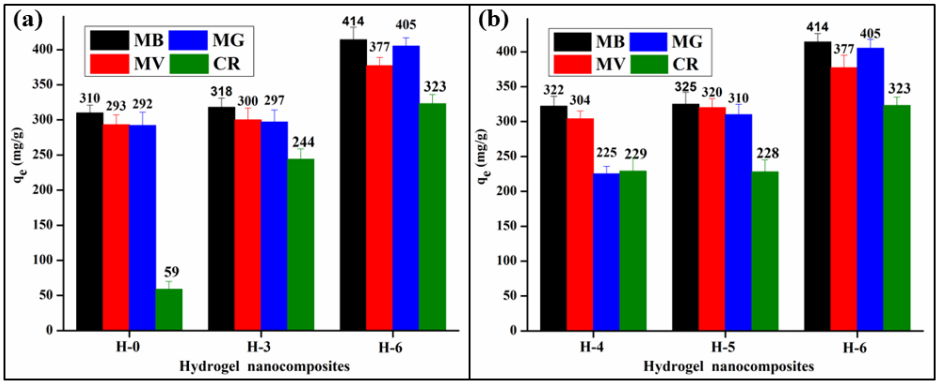

Figure 4.8. (a) Effect of CNF (0.1 wt%) and mCNF (0.1 wt%) on dye adsorption capacity of HNCs (H-0, H-3, H-6); and (b) effect of different mCNF content on dye adsorption capacity of HNCs (H-4, H-5, H-6).

Moreover, maximum value of q_e for mCNF treated hydrogel (H-6 containing 0.1 wt% mCNF) was observed higher than the H-0 and H-3 samples and also this value was observed increasing with the increase in mCNF content from 0.01 to 0.1 wt% (**Figure 4.8.b**). Particularly, q_e value of H-6 attained removal capacity of 414±20, 377±18,

405±20 and 323±16 $mg \cdot g^{-1}$ for MB, MV, MG and CR, respectively. This behavior can be ascribed to the increase in the carboxylate groups in the hydrogel matrix due to the incorporation of mCNF which can generate additional electrostatic sites between the cationic reactive sites of MB, MV, MG and CR dyes and the anionic group of mCNF, AA and IA present in the hydrogel network structure [27]. From **Figure 4.8.a**. and **Figure 4.8.b**, the highest q_e value was observed for H-6, therefore, further dye adsorption studies were conducted using this composition only.

4.3.3.7.1. Effect of contact time

To understand the effectiveness of an adsorbent, the time required for complete adsorption of dyes plays a significant role. Therefore, effect of contact time on removal of MB, MG, MV and CR dyes onto H-6 hydrogel under given conditions, such as at room temperature, an adsorbent dosage of 10 mg, and an initial concentration of 50 ppm, was investigated and the results are depicted in **Figure 4.9.a**. From the figure, it was found that the q_e value is significantly dependent on the contact time and showed similar trends of adsorption for all the dyes. Initially, dye adsorption capacity increased quickly with increasing time and then leveled off once the equilibrium was reached. This may be ascribed to the decreasing number of dye molecules in the solution with increasing contact time due to transferring of dye molecules from solution to the hydrogel network [27]. According to **Figure 4.9.a**, it can be concluded that the removal of MB, MG, MV and CR increased rapidly during the first 20 min and then, it reached q_e values within 120 min in each case of the dye [11].

4.3.3.7.2. Effect of adsorbent dosages

In adsorption process, a material can be considered as an excellent adsorbent if it can be able to remove significant amounts of pollutants at lower amounts of doses. Therefore, effect of adsorbent dosage on removal of MB, MG, MV and CR dyes was studied using different amounts of H-6 hydrogel. Using 10 - 40 mg of the hydrogel, the effect of the adsorbent dose was examined. It was found that the q_e value of H-6 decreases with the increase in amount of adsorbent dose, as shown in **Figure 4.9.b**. When the adsorbent dosage gradually increases from 10 to 40 mg, the q_e values of H-6 for the removal of MB, MG, MV and CR dyes decrease from 414±20, 377±18, 405±20 and 323±16 mg/g to 110±5, 111±6, 109±5 and 76±4 mg/g, respectively. This may be due to the presence of excessive adsorption sites when the amount of adsorbent dose was increased, which in

turn exceed the dye removal capacity for the same initial amount of dye [28]. Therefore, adsorbent dose of 10 mg was considered as an optimal dose condition.

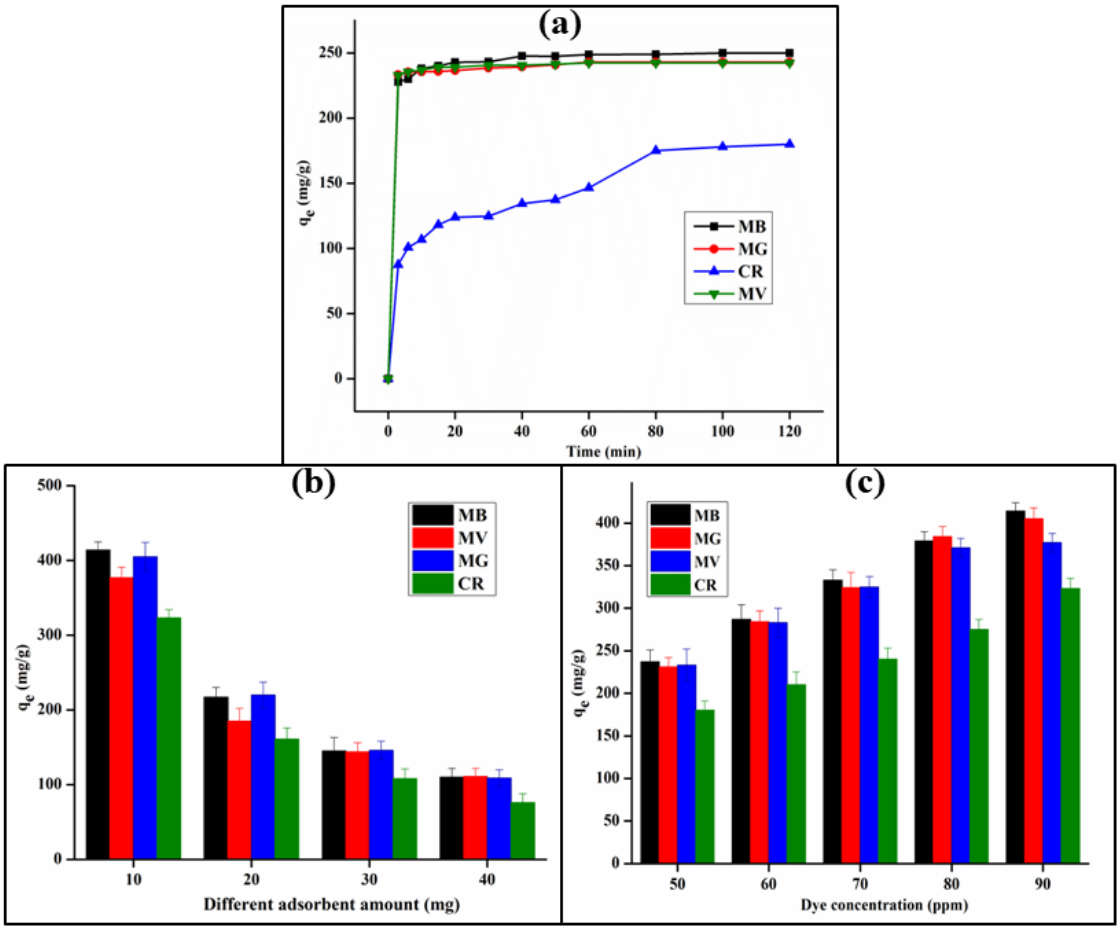

Figure 4.9. Effect of (a) contact time, (b) adsorbent dose and (c) initial dye concentration on dye adsorption capacity towards MB, MV, MG and CR of H-6 hydrogel.

4.3.3.7.3. Dye concentration

Since the initial concentration of dyes affects the q_e value of the adsorbent, so effect of concentration of MB, MG, MV and CR dyes on the q_e value of H-6 adsorbent was studied and is depicted in **Figure 4.9.c**. According to this figure, the q_e value of the adsorbent for MB, MG, MV and CR dyes increases from 237±12 to 414±20 mg/g, 231±12 to 405±20 mg/g, 233±12 to 377±18 mg/g and 180±9 to 323±16 mg/g, respectively with the increase in dye concentration from 50 to 90 ppm. This increase can be attributed to mass transfer phenomena and difference in chemical potential between the solution of dye and adsorbent surface. As the concentration of dyes increases, a strong driving force is generated due to the presence of concentration gradient between dye solution and surface of adsorbent, which in turn leads to the transfer of more dye molecules from the solution to the surface-active center of the adsorbent.

4.3.3.8. Kinetic study

To study the kinetics of adsorption and to comprehend the mechanism of adsorption of MB, MG, MV and CR dyes onto H-6 hydrogel, the experimental data were used to analyze the PFO and PSO equations. The linear plots of PFO and PSO kinetic models for MB, MG, MV and CR were presented in **Figure 4.10**.(**a** and **b**) and kinetic parameters were calculated using Eq. (5) and Eq. (6), respectively. By comparing the correlation coefficient values, the best-fitting kinetic models that described the adsorption of MB, MG, MV and CR were identified. Based on the correlation coefficient (R^2), the PSO was higher (0.999) than that of the PFO in the case of all the four dyes sample. These findings suggest that the adsorption of MB, MG, MV and CR dyes by the H-6 adsorbents was mainly dominated by electrostatic interactions between the adsorbate and adsorbent [11].

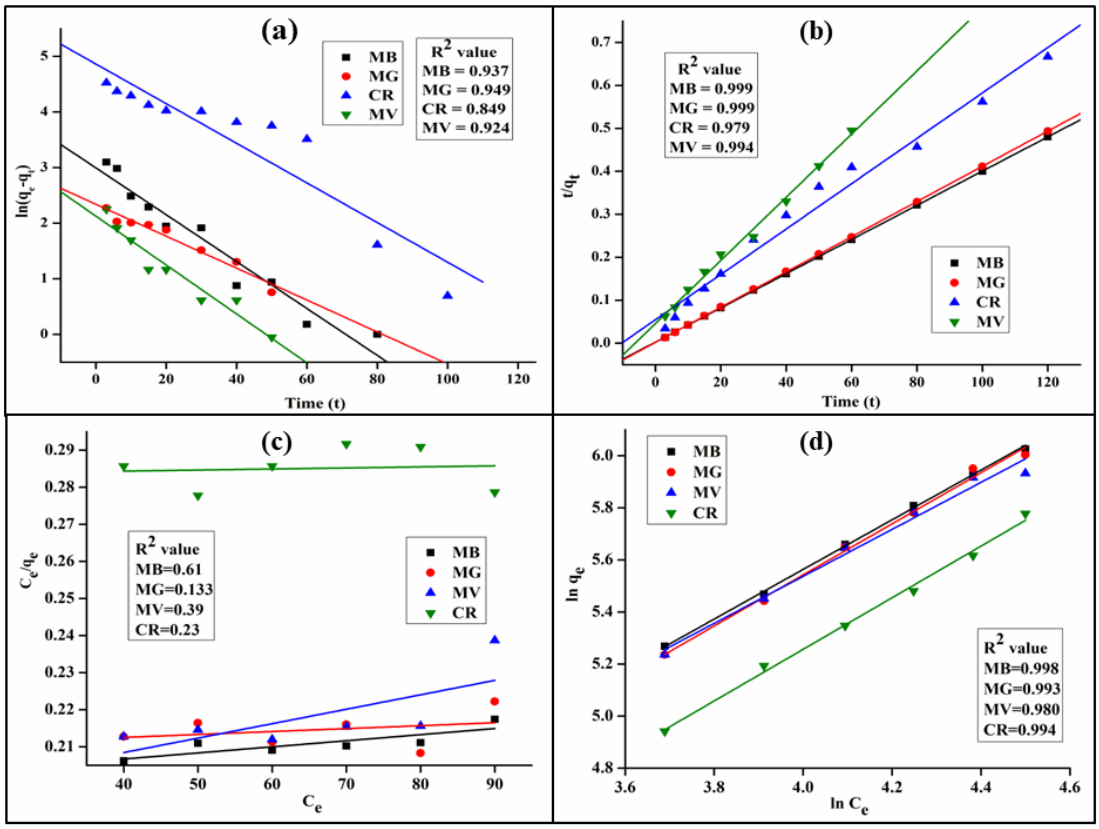

Figure 4.10. Linear plots of (a) PFO and (b) PSO kinetic equations. Linear plots of (c) Langmuir and (d) Freundlich adsorption isotherms.

4.3.3.9. Adsorption isotherm study

Adsorption isotherms are important to comprehend what type of interaction occurs between adsorbent and adsorbate. Moreover, it provides information regarding distribution of adsorbate between the adsorbent and solution phase in the adsorption

process. In this study, two models i.e., Langmuir and Freundlich isotherms were investigated to understand the adsorption isotherms. The linear fittings of these isotherm models are displayed in **Figure 4.10.c** and **d**, respectively. From the visual observation of the plots in **Figure 4.10.(c** and **d**), and the correlation coefficient (R^2), it can be confirmed that the isotherm data for H-6 are better explained by the Freundlich model and the adsorption of MB, MG, MV and CR dyes which indicates the presence of multilayer adsorption process on heterogeneous surface of H-6 hydrogel [11].

4.3.3.10. Mixed dye adsorption study

In practical applications, adsorbent materials are often utilized in mixed dye solution. Therefore, we have performed adsorption experiment in a mixed dye system containing MB/MG/MV/CR. As shown in **Figure 4.11.a**, H-6 hydrogel can effectively adsorb all the chosen cationic dyes without exact selectivity in the mixed dye solution. Moreover, the ratios of q_e^{mix}/q_e^{mono} for the dyes were also determined which was found to be less than 1. This is attributable to the presence of other dye molecules which prevent each other from adsorption on the surface of adsorbent [12].

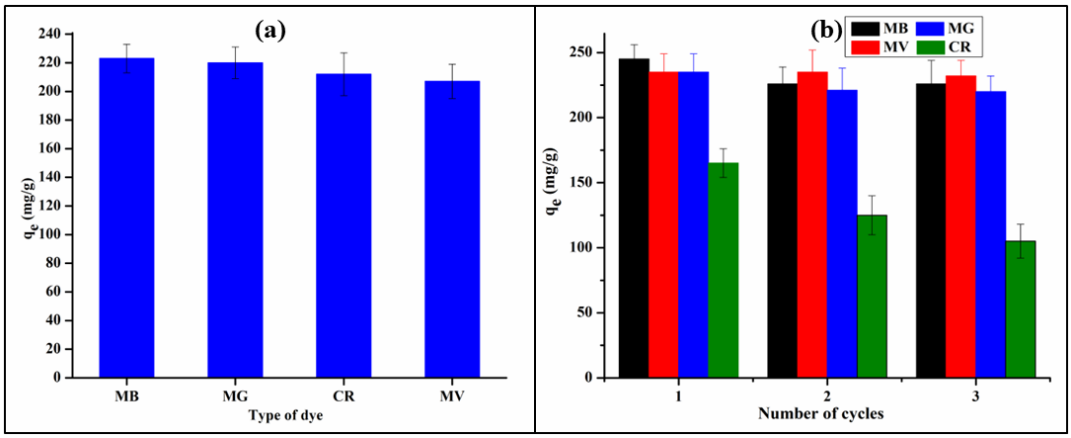

Figure 4.11. (a) Adsorption capacity of HCN adsorbent (H-6) in mixed dye solution and (b) its reusability up to three cycles towards different cationic dyes.

4.3.3.11. Desorption and dye re-adsorption experiment

It is crucial to regenerate the utilized adsorbent after the adsorption process. Considering industrial application, regeneration/reusability are the prime factors for pollutant removal process. Therefore, adsorbent should possess excellent reusable property without remarkable loss in its affinity towards pollutants. So to illustrate the reusability of the prepared adsorbent, three consecutive adsorption/desorption cycles were carried out under the identical conditions. It was observed that adsorbed dye molecules could be

effectively removed from the adsorbent by using the method described in earlier section. As shown in **Figure 4.11.b**, only a slight reduction in q_e value of the hydrogel was observed even after three cycles of adsorption/desorption process, which indicate that the hydrogel provides strong electrostatic interaction which can be used for several times. However, the observed slight decrease in q_e value after 3 cycles can be attributed to weight loss of the hydrogel adsorbent due to its successive washing processes. Moreover, a difference in removal capacity was observed in this experiment, indicating that the prepared hydrogel exhibits a different affinity for CR compared with other cationic dyes. This might be due to the presence of stronger electrostatic interactions between CR and the hydrogel matrix, so that residual dye molecules occupy the active sites, leading to a decrease in adsorption capacity after each cycle. From these results, we can conclude that the hydrogel possesses excellent recyclable property towards the removal of cationic dyes **[**29].

4.4. Conclusion

In this work, we have fabricated HNCs with incorporation of mCNF via the free radical polymerization reaction and it was used as adsorbent for removal of MB, MG, MV and CR from aqueous solutions. From FTIR, TGA, XRD, TEM, DLS and SEM studies of NMs and HNCs, formation of CNF, mCNF and HNCs were confirmed. The results of experimental studies showed that WAC and q_e of H-6 increases with the increase in content of mCNF from 0.01 to 0.1%. The maximum WAC was found to be 754 g/g and the highest dye removal capacity was observed to be 414±20, 377±18, 405±20 and 323±16 mg/g for MB, MG, MV and CR dyes, respectively. Moreover, kinetic and isotherm studies were in agreement with PSO and Freundlich isotherm, respectively. Further, mixed dye adsorption and reusability test of H-6 hydrogel indicated that the hydrogel could effectively be adsorbed dyes from the mixture of dyes, and it could be efficiently reused for dye adsorption up to three adsorption/desorption cycles. Based on these studies, it can be concluded that the prepared biobased HNC might be used as an effective and reusable adsorbent for removal of dyes from wastewater.

References

[1] Zhou, C., Wu, Q., Lei, T., and Negulescu, I. I. Adsorption kinetic and equilibrium studies for methylene blue dye by partially hydrolyzed polyacrylamide/cellulose

nanocrystal nanocomposite hydrogels. *Chemical Engineering Journal,* 251:17-24, 2014.

[2] Abdelrahman, E. A., Hegazey, R. M., and El-Azabawy, R. E. Efficient removal of methylene blue dye from aqueous media using Fe/Si, Cr/Si, Ni/Si, and Zn/Si amorphous novel adsorbents. *Journal of Materials Research and Technology,* 8:5301-5313, 2019.

[3] Baghbadorani, N. B., Behzad, T., Etesami, N., and Heidarian, P. Removal of Cu^{2+} ions by cellulose nanofibers assisted starch-graft-poly(acrylic acid) superadsorbent hydrogels. *Composites Part B: Engineering,* 176:107084, 2019.

[4] Wang, W., Kang, Y., and Wang, A. One-step fabrication in aqueous solution of a granular alginate-based hydrogel for fast and efficient removal of heavy metal ions. *Journal of Polymer Research,* 20:1-10, 2013.

[5] Husnaini, S., Hanisah, N., Suhaili, N., Hannan, F., Mat, A., and Othaman, R. Preparation of cellulose-based hydrogel : A review. *Journal of Materials Research and Technology,* 10:935–952, 2020.

[6] Deepa, B., Abraham, E., Cordeiro, N., Mozetic, M., Mathew, A. P., Oksman, K., Faria, M., Thomas, L., and Pothan, L. A. Utilization of various lignocellulosic biomass for the production of nanocellulose: A comparative study. *Cellulose,* 22:1075-1090, 2015.

[7] Safarzadeh, H., Peighambardoust, S. J., and Peighambardoust, S. H. Application of a novel sodium alginate-graft-poly(methacrylic acid-co-acrylamide)/ montmorillonite nanocomposite hydrogel for removal of malachite green from wastewater. *Journal of Polymer Research*, 30:157, 2023.

[8] Mandal, A. and Chakrabarty, D. Isolation of nanocellulose from waste sugarcane bagasse (SCB) and its characterization. *Carbohydrate Polymers,* 86:1291-1299, 2011.

[9] Alam, M. N., Islam, M. S., and Christopher, L. P. Sustainable production of cellulose-based hydrogels with superb absorbing potential in physiological saline. *ACS Omega,* 4: 9419-9426, 2019.

[10] Rahman, M. M., Alam, M., Rahman, M. M., Susan, M. A. B. H., Shaikh, M. A. A., Nayeem, J., and Jaha, M. S. A novel approach in increasing carboxymethylation reaction of cellulose. *Carbohydrate Polymer Technologies and Applications,* 4:100236, 2022.

[11] Allouss, D., Essamlali, Y., Amadine, O., Chakir, A., Zahouily, M. Response surface methodology for optimization of methylene blue adsorption onto carboxymethyl cellulose-based hydrogel beads: Adsorption kinetics, isotherm, thermodynamics and reusability studies. *RSC Advances,* 9:37858-37869, 2019.

[12] Godiya, C. B., Sayed, S. M., Xiao, Y., and Lu, X. Highly porous egg white/polyethyleneimine hydrogel for rapid removal of heavy metal ions and catalysis in wastewater. *Reactive and Functional Polymers,* 149:104509, 2020.

[13] Palanichamy, P., Venkatachalam, S., and Gupta, S. Improved recovery of cellulose nanoparticles from printed wastepaper and its reinforcement in guar gum films. *Biomass Conversion and Biorefinery,* 1-13, 2022.

[14] de Souza, A. G., Rocha, D. B., Kano, F. S., and dos Santos Rosa, D. Valorization of industrial paper waste by isolating cellulose nanostructures with different pretreatment methods. *Resources, Conservation and Recycling,* 143:133-142, 2019.

[15] Brännvall, E. and Aulin, C. CNFs from softwood pulp fibers containing hemicellulose and lignin. *Cellulose*, 29:4961-4976, 2022.

[16] Farooq, A., Li, M., Alasood, A., Farooq, A., Ashraf, M., Patoary, M. K., and Liu, L. Novel pretreatment performance evaluation for cellulose nanofibrils extraction from ficus natalensis barkcloth. *Journal of Polymers and the Environment,* 30:1547–1559, 2022.

[17] Huang, D., Hong, H., Huang, W., Zhang, H., and Hong, X. Scalable preparation of cellulose nanofibers from office waste paper by an environment friendly method. *Polymers*, 13:3119, 2021.

[18] Zhou, Y., Fu, S., Zhang, L., and Zhan, H. Superabsorbent nanocomposite hydrogels made of carboxylated cellulose nanofibrils and CMC-g-(AA-co-AM). *Carbohydrate Polymers*, 97:429-435, 2013.

[19] Olad, A., Doustdar, F., and Gharekhani, H. Fabrication and characterization of a starch-based superabsorbent hydrogel composite reinforced with cellulose nanocrystals from potato peel waste. *Colloids and Surface A: Physicochemical and Engineering Aspects*, 601:124962,2020.

[20] Chen, J., Li, H., Fang, C., Cheng, Y., Tan, T., and Han, H. Synthesis and structure of carboxymethylcellulose with a high degree of substitution derived from waste disposable paper cups. *Carbohydrate Polymers*, 237:116040, 2020.

[21] Li, J., Dong, Y., Hu, L., Zhang, Y., Fu, Q., Zhang, L., Zhu, X., and Liao, Q. Microalgae hydrogel-derived monolithic free-standing air cathode for microbial fuel cells: Tailoring the macroporous structure for enhanced bioelectricity generation. *Renewable and Sustainable Energy Reviews,* 153:111773, 2022.

[22] Bunmechimma, L., Leejarkpai, T., and Riyajan, S. A. Fabrication and physical properties of a novel macroporous poly(vinyl alcohol)/cellulose fibre product. *Carbohydrate Polymers*, 240:116215, 2020.

[23] Guo, X., Wang, Y., Ren, Y., and Liu, X. Fabrication of flame retardant lyocell fibers based on carboxymethylation and aluminum ion chelation. *Cellulose*, 28:6679-6698, 2021.

[24] Tudorachi, N., Lipsa, R., and Mustata, F. R. Thermal degradation of carboxymethyl starch–g-poly(lactic acid) copolymer by TG–FTIR–MS analysis. *Industrial and Engineering Chemistry Research,* 51:15537-15545, 2012.

[25] Saberi, A., Alipour, E., and Sadeghi, M. Superabsorbent magnetic Fe_3O_4-based starch-poly(acrylic acid) nanocomposite hydrogel for efficient removal of dyes and heavy metal ions from water. *Journal of Polymer Research,* 26:1-14, 2019.

[26] Zhang, D., Ren, B., Zhang, Y., Xu, Li., Huang, Q., He, Y., Li, X., Wu, J., Yang, J., Chen, Q., Chang, Y., and Zheng, J. From design to applications of stimuli-responsive hydrogel strain sensors. *Journal of Materials Chemistry B,* 8:3171-3191, 2020.

[27] Thamer, B. M., Aldalbahi, A., Moydeen, A. M., and El-Newehy, M. H. In situ preparation of novel porous nanocomposite hydrogel as effective adsorbent for the removal of cationic dyes from polluted water. *Polymers*, 12:3002, 2022.

[28] Malatji, N., Makhado, E., Ramohlola, K. E., Modibane, K. D., Maponya, T. C., Monama, G. R., and Hato, M. J. Synthesis and characterization of magnetic clay-based carboxymethyl cellulose-acrylic acid hydrogel nanocomposite for methylene blue dye removal from aqueous solution. *Environmental Science and Pollution Research,* 27:44089-44105, 2020.

[29] Naushad, M., Ahamad, T., AlOthman, Z. A., and Ala'a, H. Green and eco-friendly nanocomposite for the removal of toxic Hg (II) metal ion from aqueous environment: Adsorption kinetics and isotherm modelling. *Journal of Molecular Liquids,* 279:1-8, 2019.